Mechanisms for low-frequency variability of summer Arctic sea ice extent

Rong Zhang[1]

Geophysical Fluid Dynamics Laboratory, National Oceanic and Atmospheric Administration, Princeton, NJ 08540

Edited by John M. Wallace, University of Washington, Seattle, WA, and approved March 4, 2015 (received for review November 21, 2014)

Satellite observations reveal a substantial decline in September Arctic sea ice extent since 1979, which has played a leading role in the observed recent Arctic surface warming and has often been attributed, in large part, to the increase in greenhouse gases. However, the most rapid decline occurred during the recent global warming hiatus period. Previous studies are often focused on a single mechanism for changes and variations of summer Arctic sea ice extent, and many are based on short observational records. The key players for summer Arctic sea ice extent variability at multidecadal/centennial time scales and their contributions to the observed summer Arctic sea ice decline are not well understood. Here a multiple regression model is developed for the first time, to the author's knowledge, to provide a framework to quantify the contributions of three key predictors (Atlantic/Pacific heat transport into the Arctic, and Arctic Dipole) to the internal low-frequency variability of Summer Arctic sea ice extent, using a 3,600-y-long control climate model simulation. The results suggest that changes in these key predictors could have contributed substantially to the observed summer Arctic sea ice decline. If the ocean heat transport into the Arctic were to weaken in the near future due to internal variability, there might be a hiatus in the decline of September Arctic sea ice. The modeling results also suggest that at multidecadal/centennial time scales, variations in the atmosphere heat transport across the Arctic Circle are forced by anticorrelated variations in the Atlantic heat transport into the Arctic.

Arctic sea ice | internal variability | ocean heat transport

Observations reveal multidecadal variations in Arctic surface air temperature (SAT), and amplified Arctic warming similar to that observed in recent decades also occurred during 1930–1940 (1–3). Both observations and climate modeling results suggest that the reduced Arctic sea ice is crucial for the early twentieth century Arctic warming, and internal variability is a very likely cause for that event (3). In recent decades, satellite observations reveal a substantial decline in September Arctic sea ice extent (4). This observed recent Arctic sea ice decline is also found to have played a leading role in causing the observed amplified Arctic surface warming in recent decades (5, 6).

The summer Arctic was projected to become ice-free within a few decades by some climate models used in Coupled Model Intercomparison Project Phase 5 (CMIP5) due to the increase in anthropogenic greenhouse gases (7, 8), or even within the next decade if extrapolating the observed trend (9). These future projections imply enormous social and economic impacts, such as the potential for trans-Arctic shipping. However, the most rapid decline in summer Arctic sea ice actually occurred during the recent global warming hiatus period. The CMIP5 multimodel mean response to changes in anthropogenic radiative forcings exhibits much less decline in September Arctic sea ice extent (SIE) but stronger warming in global mean surface temperature than that observed over the recent hiatus period (10), implying that natural variability might have played an important role in the observed recent decline in September Arctic SIE.

Various mechanisms have been proposed separately for the observed recent summer Arctic sea ice decline, such as the positive ice infrared feedback, i.e., enhanced downward longwave radiative flux due to increased air temperature, water vapor, cloudiness, and reduced sea ice (11, 12); the positive ice albedo feedback (13–15); the warming of the Atlantic water in the Arctic (16–18); the increase in Bering Strait ocean heat fluxes (19); the influence of wind forcing over the central Arctic associated with the Arctic Oscillation (AO) (20, 21) and the nonlinear positive feedback (22) among Pacific inflow, Beaufort Gyre (23), and AO at interannual time scale; and the interaction between the Arctic Dipole (AD) and transpolar ice drift (24–28). The previous studies are often based on short observational records. Some crucial questions remain unknown, e.g., what are the key players for internal variability of summer Arctic SIE at multidecadal/centennial time scales and how do they contribute to the observed summer Arctic SIE decline?

Multidecadal internal variability has been observed in the Atlantic (29), and climate models suggest that the Atlantic Meridional Overturning Circulation (AMOC) variability is a major source for the Atlantic multidecadal variability (AMV) and might be important for the observed opposite trends in Arctic and Antarctica sea ice (30). Both modeling results (31, 32) and multicentury historical records (33) showed that winter Arctic sea ice variability is closely linked to the AMV. The AMOC is suggested to have strengthened since the mid 1970s as implied indirectly by its fingerprints (34, 35). Could a strengthened AMOC have led to an enhanced Atlantic heat transport into the Arctic and thus contributed to the observed recent summer Arctic SIE decline? If the AMOC and the associated Atlantic heat transport into the Arctic were to weaken in the near future due to internal variability, would there be a hiatus in the decline of September Arctic SIE and a delay in attaining a summer ice-free Arctic?

Motivated by the above questions, this paper investigates the internal low-frequency variability of summer Arctic SIE, using a 3,600-y segment of a control simulation from a renowned climate model, Geophysical Fluid Dynamics Laboratory (GFDL) Coupled Model version 2.1 (CM2.1) (36). Three key predictors for internal low-frequency variability of summer Arctic SIE are identified, and they cover a broad range of internal variability in

Significance

The observed decline in summer Arctic sea ice has often been attributed, in large part, to the increase in greenhouse gases. However, the contributions from internal low-frequency variability in the climate system are not well understood. Here a multiple regression model is developed for the first time, to the author's knowledge, to quantify the contributions of three key predictors on the internal low-frequency variability of summer Arctic sea ice extent. If the ocean heat transport into the Arctic were to weaken in the near future due to internal variability, there might be a hiatus in the decline of September Arctic sea ice, and a delay in attaining a summer ice-free Arctic. This plausible scenario with broad ecological and economic impacts should not be ignored.

Author contributions: R.Z. designed research, performed research, analyzed data, and wrote the paper.

The author declares no conflict of interest.

This article is a PNAS Direct Submission.

[1]Email: rong.zhang@noaa.gov.

This article contains supporting information online at www.pnas.org/lookup/suppl/doi:10.1073/pnas.1422296112/-/DCSupplemental.

the climate system, including both the Atlantic and Pacific ocean heat transport into the Arctic, as well as the atmosphere circulation. A multiple regression model is developed to provide a framework to quantify the contributions of the three key predictors. The advantage of such a long control simulation is the statistical reliability, especially at multidecadal/centennial time scales, which cannot be obtained by short observational records. The estimated contributions of these key predictors to the observed summer Arctic SIE decline are also discussed.

Multiple Regression and Spatial Pattern

In this paper, the low-frequency variability refers to the variability at multidecadal/centennial time scales; thus all simulated time series discussed here are 30-y low-pass filtered (LF). At multidecadal/centennial time scales, three key predictors are significantly anticorrelated with September Arctic SIE anomalies in GFDL CM2.1 control simulation (Fig. 1 *A*–*C*): (*i*) anomalous annual mean northward Atlantic heat transport across the Arctic Circle (HT_{ATL}) ($r = -0.50$ at 2-y lead), (*ii*) anomalous annual mean northward Pacific heat transport across the Arctic Circle (HT_{PAC}) ($r = -0.51$ at 2-y lead), and (*iii*) anomalous spring Arctic Dipole (AD) ($r = -0.37$ at 1-y lead). The AD index is defined as the second leading mode (PC2) of spring (April–July) sea level pressure (SLP) anomalies within the Arctic Circle, as the AD's influence on September Arctic SIE is strongest in spring. Both simulated and observed positive AD patterns exhibit a positive SLP anomaly over Greenland and a negative SLP anomaly over Kara Sea/Laptev Sea (Fig. S1 *A* and *B*).

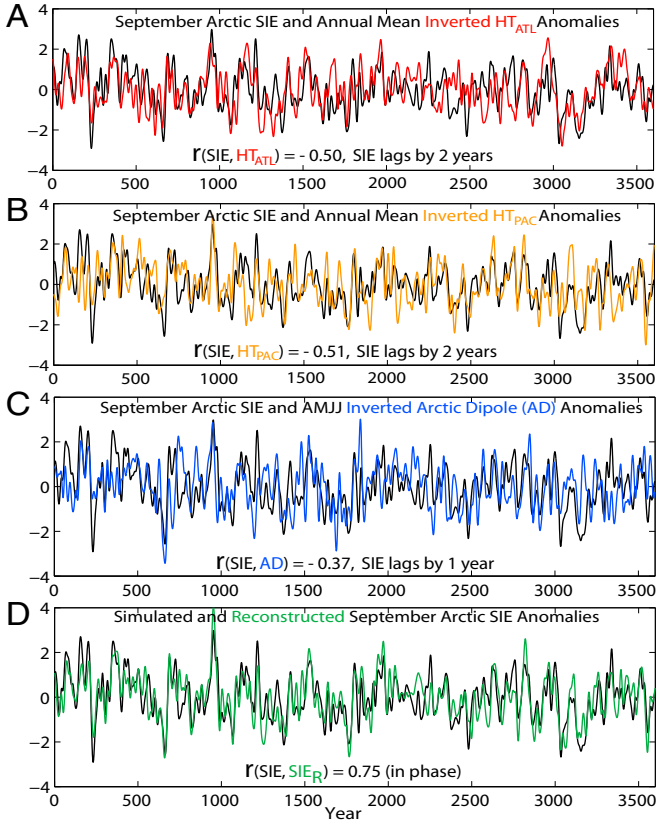

Fig. 1. Anomalies from GFDL CM2.1 control simulation. September Arctic SIE anomalies with (*A*) inverted annual mean HT_{ATL}, (*B*) inverted annual mean HT_{PAC}, (*C*) inverted spring AD, and (*D*) reconstructed September Arctic SIE anomalies. All time series are 30-y LF and normalized by corresponding SDs [$\sigma(SIE) = 0.22 \times 10^6$ km^2, $\sigma(SIE_R) = 0.17 \times 10^6$ km^2, $\sigma(HT_{ATL}) = 8.5$ TW, $\sigma(HT_{PAC}) = 0.35$ TW, $\sigma(AD) = 8.0$ hPa].

A multiple linear regression model for September Arctic SIE anomalies is derived using anomalous HT_{ATL}, HT_{PAC}, and AD as predictors (*Methods*). The September Arctic SIE anomalies reconstructed by the multiple regression model are strongly correlated with those simulated ($r = 0.75$, Fig. 1*D*), and they have significant high coherence at multidecadal/centennial time scales (Fig. S2 *A* and *B*). There is a positive correlation between HT_{PAC} and AD ($r = 0.28$ with HT_{PAC} leads AD by 1 y), and no correlation between HT_{ATL} and the other two predictors. The impacts of standardized HT_{ATL} and HT_{PAC} anomalies on summer Arctic SIE are of similar order (*Methods*). The reconstructed September Arctic SIE explains ~56% of the total variance. Various nonlinear feedbacks, such as the ice infrared feedback (11, 12) and ice albedo feedback (13–15), might contribute to the residual variance not explained by the multiple regression model.

An increase in HT_{ATL} induces reduced September sea ice concentration (SIC) at both the Atlantic and Pacific sides of the central Arctic (Fig. 2*A*), while an increasing in HT_{PAC} induces a slightly stronger (weaker) reduction of September SIC at the Pacific (Atlantic) side (Fig. 2*B*). The dipole SLP anomaly associated with the positive AD induced an enhanced transpolar wind/ice drift (Fig. 2*D*), resulting in reduced September SIC at the Pacific side but increased September SIC at the Atlantic side (Fig. 2*C*). Such opposite SIC changes lead to a smaller impact of standardized AD anomalies on September Arctic SIE than standardized HT_{ATL} and HT_{PAC} anomalies (*Methods*). A reduction in the reconstructed September Arctic SIE anomaly using all three predictors is associated with a reduction of SIC at both the Atlantic and Pacific sides (Fig. 2*E*).

At multidecadal/centennial time scales, the simulated September Arctic SIE is strongly anticorrelated ($r = -0.88$) with the simulated September Arctic SAT at zero lag, and all three key predictors for September Arctic SIE can also serve as key predictors for September Arctic SAT. This result is consistent with previous studies (3, 5, 6) that the Arctic SIE variability has a leading role in causing the Arctic SAT variability.

Mechanisms

Changes in Arctic sea ice as a whole are mainly affected directly by changes in the thermodynamic energy flux available for the melt/growth of Arctic sea ice and changes in wind forcing that can induce anomalous ice motion in the Arctic. Hence the predictors for September Arctic SIE anomalies are screened in terms of various thermodynamic and wind forcings over the Arctic that have direct causal effects on September Arctic SIE.

If we take the total sea ice mass within the Arctic Circle as a whole and ignore the sensible heat storage in ocean, land, and ice, the thermodynamic energy flux available for the net melt of annual mean Arctic sea ice mass is given by $-F_{SFC} + F_O + F_I$ (equation 8 in ref. 37). Here F_{SFC} is the annual mean net upward surface heat flux released into the atmosphere within the Arctic Circle, F_O is the annual mean poleward ocean heat transport across the Arctic Circle, and F_I is the annual mean poleward ice latent heat transport (i.e., the equatorward ice mass transport multiplied by the latent heat of fusion) across the Arctic Circle. A net outflow of ice is equivalent to an inflow of ice latent heat across the Arctic Circle. Hence the various thermodynamic forcings screened for predictors of September Arctic SIE include F_O, F_{SFC}, and F_I.

At multidecadal/centennial time scales, an enhanced F_O, such as the Atlantic heat transport, leads to a net basal melting and thus a reduction in Arctic ice mass at all seasons, and the response is strongest in Barents Sea/Greenland Sea in spring, fall, and winter and decays from the Atlantic side to the Pacific side (Figs. S3 and S4). An enhanced Pacific heat transport also leads to a reduction in Arctic sea ice mass at all seasons, and the response is strongest near the Bering Strait in spring, fall, and winter and decays from the Pacific side to the Atlantic side (Figs. S3 and S4). The F_{SFC} variability is dominated by the Atlantic heat transport variability (described in *Surface Heat Flux and Atmosphere Heat Transport*), so an enhanced F_{SFC} (i.e., a reduced

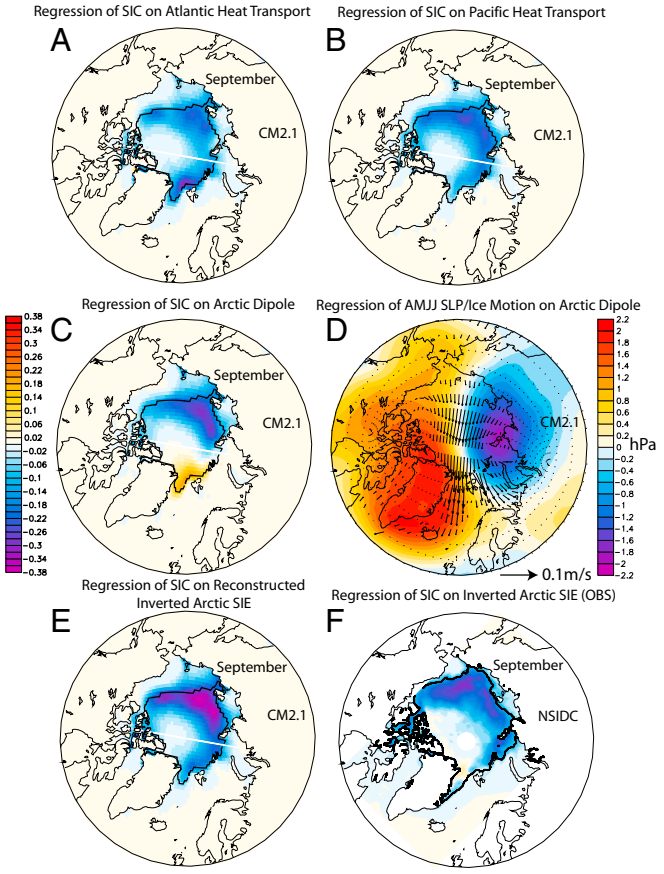

Fig. 2. Spatial pattern. (*A*–*C*) Regression of anomalous September SIC on 0.65 million km^2, 0.58 million km^2, and 0.32 million km^2 reduction of September Arctic SIE induced by anomalous HT_{ATL} (2-y lead) (*A*), HT_{PAC} (2-y lead) (*B*), and AD (1-y lead) (*C*), respectively (Eq. **2**). (*D*) Regression of anomalous April–July (AMJJ) SLP/ice motion on AD (1-y lead) as in *C*. (*E*) Regression of anomalous September SIC on 1 million km^2 reconstructed inverted September Arctic SIE anomaly (Eq. **2**). (*F*) Regression of observed anomalous September SIC on 1 million km^2 inverted observed September Arctic SIE anomaly (1979–2013). Note that *A*–*E* are LF regressions from CM2.1 and *F* is unfiltered regression from observation. Thick black lines denote climatological September ice edges. The white lines in *A*–*C* and *E* are due to the polar projection of SIC simulated on tripolar grids in CM2.1.

net downward surface heat flux $-F_{SFC}$) is associated with a reduced Arctic ice mass and provides a negative feedback. The simulated F_I variability is dominated by the ice mass variability at the Arctic Circle, and thus a reduction in F_I is associated with a reduction in Arctic ice mass and less ice outflow, also providing a negative feedback. Changes in Arctic ice mass at all seasons are highly correlated with and contribute to September Arctic SIE anomalies. Hence at multidecadal/centennial time scales, the Atlantic and Pacific heat transport act as key predictors, whereas F_{SFC} and F_I only provide negative feedbacks for September Arctic SIE changes.

The Atlantic water enters the Arctic through two main branches (Fig. 3*A*): One enters the Barents Sea through the Barents Sea Opening (BSO), the other through the Eastern Fram Strait (FSE) (38). At multidecadal/centennial time scales, the simulated HT_{ATL} anomalies lead coherent variations in northward heat transport across FSE (HT_{FSE}), eastward heat transport across BSO (HT_{BSO}), and Atlantic water temperature along BSO, by 2 y (Fig. S2 *C* and *D*). Hence September Arctic SIE anomalies are also significantly anticorrelated with HT_{FSE} ($r = -0.51$) and HT_{BSO} ($r = -0.58$), respectively, at zero lag. The simulated anomalous HT_{ATL} is mainly induced by the AMOC variability and lags it by 1 y (Fig. 3*C* and Fig. S2 *C* and *D*). The simulated anomalous HT_{PAC} is affected by the mean flow advection of anomalous temperature in summer across the Bering Strait, the only Pacific gateway to the Arctic (Fig. 3*A*), and in phase with the simulated summer Pacific Decadal Oscillation (PDO) Index at low frequency.

The various atmosphere circulation modes (wind forcing) over the Arctic screened for predictors of September Arctic SIE include AD, AO (leading mode of SLP north of 20°N), and North Atlantic Oscillation (NAO; leading mode of SLP over the North Atlantic). The simulated AD and AO patterns over the central Arctic in CM2.1 are comparable to those observed (Fig. S1). A positive AD is efficient in causing enhanced transpolar ice drift and thus a reduction in sea ice mass at the Pacific side and a slight increase in sea ice mass at the Atlantic side, with a stronger response in spring/summer and a much weaker response in fall/winter (Figs. S3 and S4). These changes in Arctic ice mass contribute to September Arctic SIE anomalies. Hence, although AD is the second leading mode in SLP, it is a key predictor for September Arctic SIE. Previous studies found that the wind forcing over the central Arctic associated with the AO is important for summer Arctic SIE variability at interannual/decadal time scales during the satellite era (20, 21). Here, at multidecadal/centennial time scales over the entire 3,600-y segment of the control simulation, the AO, which is highly correlated with the NAO, does not have much direct impact on September Arctic SIE. However, winter NAO/AO is involved indirectly through its delayed influence on the AMOC/Atlantic heat transport. Those variables having indirect causal effects on September Arctic SIE, such as AMOC, PDO, and winter NAO/AO, are not taken as predictors and do not improve the multiple regression model predictions if included, because their effects have already been represented by the Atlantic and Pacific heat transport.

Other climate models, such as National Center for Atmospheric Research (NCAR) Community Climate System Model versions 3 and 4 (CCSM3 and CCSM4), also exhibit a large spread in summer Arctic SIE anomalies among individual ensemble members under the same changes in anthropogenic forcing, indicating a strong influence of internal variability on summer Arctic SIE (28, 39, 40). The result in GFDL CM2.1 is consistent with the recent study (28) showing that the AD is very important in driving internal variability in summer Arctic SIE in NCAR CCSM3 through

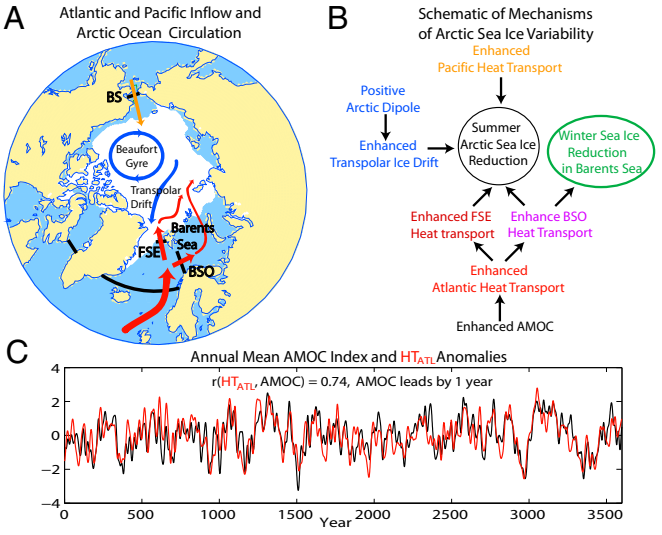

Fig. 3. Mechanisms for low-frequency variability of summer Arctic SIE. (*A*) Schematic of Atlantic/Pacific inflow (red/orange arrows) and Arctic ocean circulation. White color reflects observed climatological September SIE over 1979–2013. (*B*) Schematic of key mechanisms. (*C*) Simulated LF annual mean AMOC index and HT_{ATL} anomalies, normalized by their SDs [σ(AMOC) = 0.8 Sverdrup]. BS, Bering Strait.

its influence on the transpolar ice drift, and the spring AD has the strongest influence.

In spring, fall, and winter, the SIC anomalies within the Arctic Circle mainly appear in Barents Sea/Greenland Sea where the climatology SIC is low; thus, in these seasons, the Atlantic heat transport is the prime driver for low-frequency variability of Arctic SIE, whereas the Pacific heat transport and AD do not have much impact on Arctic SIE, although they can affect sea ice mass in the Pacific side of the central Arctic (Figs. S3 and S4). In summer, the climatology SIC is also low in the Pacific side of the central Arctic; thus summer SIC anomalies in this region are more prominent and significantly anticorrelated with the Pacific heat transport and AD as well, and the three predictors (Atlantic/Pacific heat transport and AD) are all important for summer Arctic SIE variability (Fig. 3*B*).

Surface Heat Flux and Atmosphere Heat Transport

The simulated global zonally integrated poleward ocean heat transport anomalies across the Arctic Circle are dominated by HT_{ATL} anomalies, because HT_{PAC} anomalies are negligible (Fig. 4*B*). In quasi-equilibrium at low frequency, an enhanced HT_{ATL} leads to an enhanced upward surface heat flux within the Arctic Circle (F_{SFC}) with 1-y lead (Fig. 4 *A* and *B*). Because the heat capacity of the atmosphere is very small, and the simulated increase in net upward radiative heat flux at the top-of-atmosphere is negligible, the enhanced F_{SFC} is mainly balanced by a reduced global zonally integrated northward atmospheric heat transported across the Arctic Circle (HT_{ATM}), i.e., F_{SFC} and HT_{ATM} anomalies are strongly anticorrelated at zero lag (Fig. 4*B*). Hence an enhanced Atlantic heat transport is compensated by a reduced atmosphere heat transport with 1-y lag. As a result, HT_{ATL} anomalies are not efficient for affecting summer Arctic SIE variability, and the impacts of standardized HT_{ATL} and HT_{PAC} anomalies on summer Arctic SIE variability are of similar order (*Methods*). The anticorrelation between global zonally integrated ocean and atmosphere heat transport anomalies is often referred to as Bjerknes compensation (41) and has been found at decadal time scale (42–45). Here, at multidecadal/centennial time scales, the Bjerknes compensation across the Arctic Circle is mainly between HT_{ATL} anomalies (which dominate global zonally integrated ocean heat transport anomalies) and HT_{ATM} anomalies; their anticorrelation is much higher than that at decadal time scale (Fig. 4 *C* and *D*), and changes in HT_{ATM} and F_{SFC} are forced by changes in HT_{ATL} and thus provide a negative feedback to September Arctic SIE variations.

Implications for Observed Summer Arctic Sea Ice Decline

The observed September Arctic SIE decline is associated with a decline of September SIC in the central Arctic, with a stronger decline at the Pacific side (Fig. 2*F*). This observed regression (Fig. 2*F*) is unfiltered due to the short record (1979–2013), and thus cannot be directly compared with the modeled LF regressions (Fig. 2 *A*–*E*). Modeling results (Fig. S5 *A* and *B*) show that the unfiltered regression exhibits a stronger signal at the Pacific side and a weaker signal at the Atlantic side than the LF regression. In the central Arctic, the Atlantic water is located at a deeper layer below the Pacific water; thus it takes a much longer time for the enhanced heat carried by the Atlantic water to penetrate upward to melt the central Arctic sea ice. Hence, at interannual/decadal time scales, HT_{PAC} and AD have a much higher impact on September Arctic SIE than HT_{ATL}, while, at multidecadal/centennial time scales, the impact of HT_{ATL} on September Arctic SIE greatly increases and becomes comparable to HT_{PAC} (Fig. S2*A*). The unfiltered regression using the short observed record (Fig. 2*F*) mainly reflects sea ice variations at interannual/decadal time scales, and suggests that positive HT_{PAC} and AD anomalies may have contributed to the observed stronger September SIC decline at the Pacific side of the central Arctic at interannual/decadal time scales. The impact of the enhanced HT_{ATL} on the decline of September SIC is mainly at multidecadal/centennial time scales, and thus is barely seen in the unfiltered regressions (Fig. 2*F* and Fig. S5*B*) but is more visible

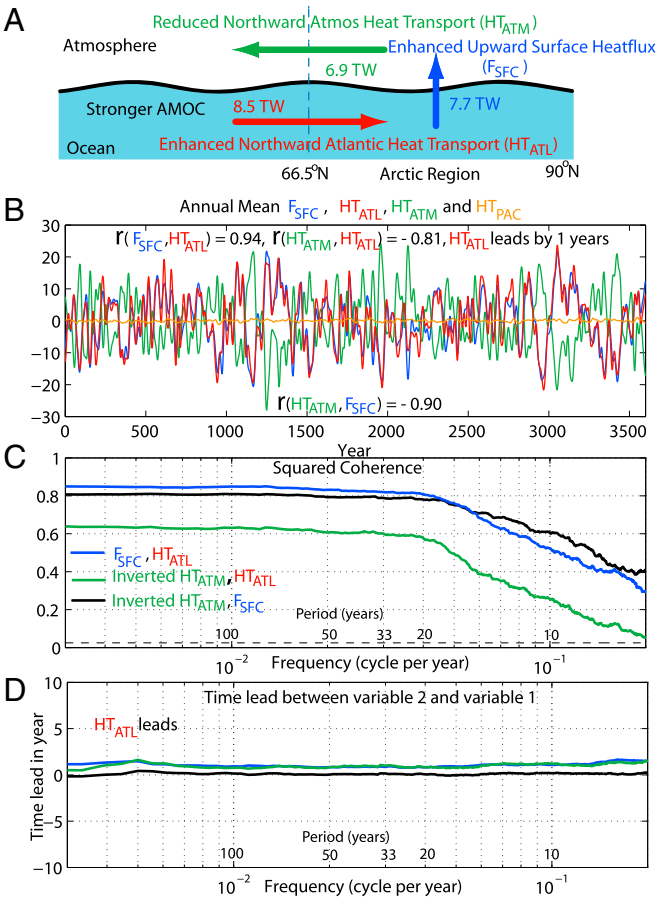

Fig. 4. Relationship among anomalous annual mean HT_{ATL}, F_{SFC}, and HT_{ATM}. (*A*) Schematic diagram. (*B*) Simulated LF annual mean F_{SFC}, HT_{ATL}, HT_{ATM}, and HT_{PAC} anomalies. (*C* and *D*) Squared coherence (*C*) and time lead (*D*) among unfiltered variables. The dashed black line in *C* is the 99% significance level.

(especially at the Atlantic side of the central Arctic) in the LF regression (Fig. S5*A*).

Both simulated and observed September SIC anomalies (Fig. 2 *E* and *F*) are close to the inner side of the climatological September ice edges in the central Arctic (except the side near Canadian Archipelago and Northern Greenland), because the September SIC at these regions with low climatology (Fig. S5 *C* and *D*) is more sensitive to changes in thermodynamic or wind forcing. GFDL CM2.1 has the least climatological mean September Arctic SIE compared with CMIP5 models (Table S1), and this bias in the climatological mean September Arctic SIE corresponds to a poleward shift of the climatological mean September ice edge in GFDL CM2.1 compared with that observed (Fig. S5 *C* and *D*). This mean state bias in GFDL CM2.1 leads to a biased poleward shift of the simulated September SIC anomalies compared with those observed (Fig. S5*B* and Fig. 2*F*). In contrast to the mean state, the simulated low-frequency variability of September Arctic SIE in GFDL CM2.1 is quite representative of those in CMIP5 models (Fig. S6 and Table S1).

The estimated contributions of the Atlantic/Pacific inflow and AD to the observed September Arctic SIE decline are discussed in the rest of this section. So far, there is no direct observation of HT_{ATL}, which requires measurements across the entire Atlantic at the Arctic Circle. However, the heat transport across the much narrower BSO (HT_{BSO}) can be measured more easily and has already been observed (46). At low frequency, the simulated HT_{BSO} dominates the anticorrelated ($r = -0.91$) March Barents Sea SIE variability (Figs. 3*B* and 5*A* and Fig. S7 *A* and *B*), and

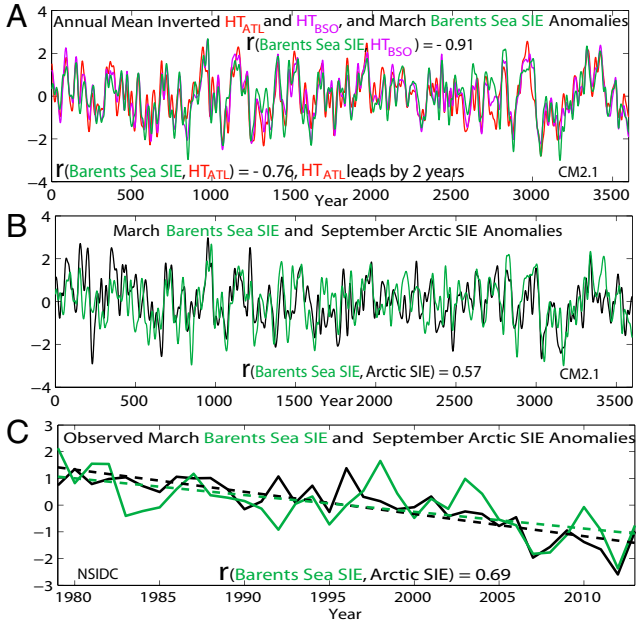

Fig. 5. Linkage with March Barents Sea SIE. (*A*) Simulated inverted LF annual mean HT_{ATL} and HT_{BSO}, and March Barents Sea SIE anomalies. (*B*) Simulated LF March Barents Sea SIE and September Arctic SIE anomalies. Time series in *A* and *B* are normalized by their SDs [$\sigma(HT_{BSO})$ = 3.0 TW, $\sigma(SIE^{March}_{Barent\ Sea})$ = 0.035 × 10^6 km^2]. (*C*) Observed September Arctic SIE and March Barents Sea SIE anomalies 1979–2013 (normalized by their SDs, 1.1 million km^2 and 0.14 million km^2, respectively).

the observed increase in HT_{BSO} is also found as a prime driver for the recent observed sea ice decline in Barents Sea (46, 47). Hence, at low frequency, the March Barents Sea SIE anomaly can be taken as a proxy for the HT_{BSO} anomaly (*Methods*). The simulated September Arctic SIE and March Barents Sea SIE anomalies have significant correlation (r = 0.57, Fig. 5*B*) and coherence (Fig. S7 *A* and *B*) at low frequency, as they are both affected by HT_{BSO}. The observed September Arctic SIE and March Barents Sea SIE also have very similar normalized decline trends from 1979 to 2013, and both have accelerated declines in the recent hiatus period and are highly correlated (r = 0.69, Fig. 5*C*), indicating the important role of the Atlantic inflow. The HT_{BSO} is estimated to have a long-term increasing trend of ∼8.4 TW/decade from 1979 to 2013 (*Methods*) thus have contributed ∼37% of the observed September Arctic SIE decline trend (1979–2013), using the simulated simple regression coefficient between 35-y trends of September Arctic SIE and HT_{BSO} (Table S2). Here the regression on HT_{BSO} represents the net effect of the Atlantic inflow on September Arctic SIE, i.e., it also includes the impact of HT_{FSE} which varies coherently with HT_{BSO} (r = 0.83, Fig. S7 *C* and *D*).

The observed AD index has an increasing trend of 10.7 hPa/decade (1979–2013). This corresponds to a positive trend of 1.1 hPa over Greenland and a negative trend of 2.1 hPa over Kara Sea/Laptev Sea in spring SLP over the 35-y period, when multiplied by the AD pattern (Fig. S1*B*). The observed AD anomaly is anticorrelated with the observed September Arctic SIE anomaly (r = −0.53, Fig. S8). The observed positive AD trend is estimated to have induced ∼12% of the observed September Arctic SIE decline trend (1979–2013), using the simulated simple regression coefficient between 35-y trends of September Arctic SIE and AD (Table S2). Since the two predictors (HT_{BSO} and AD) are independent from each other, together, they have contributed ∼49% of the observed September Arctic SIE decline trend (1979–2013), i.e., about half of the observed September Arctic SIE decline trend since 1979 might be due to internal variability.

The trend of HT_{PAC} from 1979 to 2013 is unknown, but HT_{PAC} has an observed increasing trend of ∼4 TW/decade from 2001 to 2011 (19) and is estimated to have contributed ∼44% of the observed decline trend in September Arctic over this global warming hiatus period, using the simulated simple regression coefficient between 11-y trends of September Arctic SIE and HT_{PAC} (Table S2). This is also consistent with the observed rapid sea ice decline at the Pacific side of the central Arctic during the recent hiatus period.

The above estimates suggest that internal variability associated with the three key predictors could have contributed substantially to the observed summer Arctic sea ice decline. Hence internal variability could be as important as anthropogenic forcing in the observed summer Arctic sea ice decline, and simply extrapolating the short observed sea ice decline would overestimate future changes. There might be a hiatus in summer Arctic sea ice decline if internal variations were to reverse in the near future.

Discussion

The modeling results here suggest that, to predict future summer Arctic SIE variations, it is important to monitor internal variability associated with the three key predictors (Atlantic/Pacific heat transport into the Arctic, and Arctic Dipole), in addition to the focus on anthropogenic changes. The observed summer Arctic SIE decline is outside the simulated range in most coarse-resolution models forced with anthropogenic changes (7, 10, 48), and this might be partially due to a plausible underestimation of internal variability in these models. It might be useful to use high-resolution models to improve simulated changes in the Atlantic/Pacific heat transport into the Arctic to reinvestigate the role of internal variability and accurately project future changes in Arctic sea ice. In both modeling results and observations, the September Arctic SIE variations are significantly correlated with March Barents Sea SIE variations, indicating the important role of the Atlantic heat transport into the Arctic. The estimated increase in the Atlantic heat transport into the Arctic since 1979 is consistent with the strengthening of AMOC since the mid 1970s implied by indirect evidence such as the AMOC fingerprints (34, 35), and could have contributed substantially to the observed summer Arctic SIE decline. If the AMOC and the associated Atlantic heat transport into the Arctic were to weaken in the near future due to internal variability, there might be a hiatus in the decline of September Arctic SIE, and a delay in attaining a summer ice-free Arctic.

Methods

The observed SIE and SIC are taken from National Snow and Ice Data Center (NSIDC) satellite data (49, 50) for the period 1979–2013. The Arctic SIE is defined as the total marine area within the Arctic Circle (66.5°N) with SIC of at least 15%, and the Barents Sea SIE is defined as the total marine area within the Barents Sea with SIC of at least 15%. The climatological September ice edge is where the climatological September SIC drops below 15%. The observed SLP data are from National Centers for Environmental Prediction (NCEP)/NCAR Reanalysis (51) for the period 1948–2013. The GFDL CM2.1 control simulation used in this study has fixed radiative forcings at year 1860's level (34), and the simulated AMOC exhibits variability at decadal (35) and centennial (52) time scales. The AMOC index is defined as the maximum annual mean Atlantic meridional overturning streamfunction at 45°N in density space. The simulated summer PDO Index is defined as the leading mode in summer North Pacific sea surface temperature. A multiple linear regression model for the 30-y LF September Arctic SIE anomalies is derived using three LF predictors (HT_{ATL}, HT_{PAC}, and AD):

$$SIE(t) = \beta_{ATL} HT_{ATL}(t-\tau_{ATL}) + \beta_{PAC} HT_{PAC}(t-\tau_{PAC}) + \beta_{AD} AD(t-\tau_{AD}) + \varepsilon = SIE_R(t) + \varepsilon \quad [1]$$

where the regression coefficients, $\beta_{ATL} \approx -0.013 \times 10^6$ km^2/TW, $\beta_{PAC} \approx -0.28 \times 10^6$ km^2/TW, and $\beta_{AD} \approx -0.0067 \times 10^6$ km^2/hPa, are derived from the least square best fit. Each predictor is selected at the time lead τ when it has the maximum anticorrelation with September Arctic SIE. Here $\tau_{ATL} \approx 2$ y,

$\tau_{PAC} \approx 2$ y, $\tau_{AD} \approx 1$ y, and ε is noise. The reconstructed September Arctic SIE anomalies, $SIE_R(t)$, and the predictors can be normalized by their SDs,

$$\frac{SIE_R(t)}{\sigma(SIE_R)} = -0.65\frac{HT_{ATL}(t-2)}{\sigma(HT_{ATL})} - 0.58\frac{HT_{PAC}(t-2)}{\sigma(HT_{PAC})} - 0.32\frac{AD(t-1)}{\sigma(AD)}. \quad [2]$$

In addition, the March Barents Sea SIE anomaly can be taken as a proxy for the HT_{BSO} anomaly through a simple regression at low frequency,

$$SIE^{March}_{Barents\ Sea}(t) = \alpha_{BSO} HT_{BSO}(t) + \varepsilon. \quad [3]$$

The least square slope between 35-y trends of HT_{BSO} and March Barents Sea SIE is $\alpha_{BSO} \approx -0.0107$ million km^2/TW. The HT_{BSO} is estimated to have increased 20TW from 1979 to 2007 (46), and the observed March Barents Sea SIE has decreased 0.21 million km^2 over the same period, resulting in $\alpha_{BSO} \approx -0.0105$ million km^2/TW, similar to that found in GFDL CM2.1. The HT_{BSO} is estimated to have a long-term increasing trend of ~8.4 TW/decade from 1979 to 2013, given the observed long-term decline trend in March Barents Sea SIE (0.09×10^6 km^2/decade) over the same period and CM2.1 derived slope α_{BSO}.

The predictors in the regression models refer to anomalies with zero mean, and all regression models are tested with double cross-validation and are robust due to the very large sample size. The maximum anticorrelation between each of the three predictors and September Arctic SIE at the corresponding time lead is significant at the corresponding 99% level using both the two-tailed Student's *t* test and the Monte Carlo test.

ACKNOWLEDGMENTS. I thank Kirk Bryan, Matthew Harrison, Isaac Held, Thomas Knutson, and Michael Winton for discussions of the paper, and the three anonymous reviewers for the very helpful comments.

1. Polyakov IV, et al. (2003) Variability and trends of air temperature and pressure in the maritime Arctic, 1875–2000. *J Clim* 16(12):2067–2077.
2. Semenov VA, Bengtsson L (2003) Modes of the wintertime Arctic temperature variability. *Geophys Res Lett* 30(15):1781.
3. Bengtsson L, Semenov VA, Johannessen OM (2004) The early twentieth-century warming in the Arctic—A possible mechanism. *J Clim* 17(20):4045–4057.
4. Comiso JC, Parkinson CL, Gersten R, Stock L (2008) Accelerated decline in the Arctic sea ice cover. *Geophys Res Lett* 35(1):L01703.
5. Serreze MC, Barrett AP, Stroeve JC, Kindig DN, Holland MM (2009) The emergence of surface-based Arctic amplification. *Cryosphere* 3:11–19.
6. Screen JA, Simmonds I (2010) The central role of diminishing sea ice in recent Arctic temperature amplification. *Nature* 464(7293):1334–1337.
7. Stroeve JC, et al. (2012) Trends in Arctic sea ice extent from CMIP5, CMIP3 and observations. *Geophys Res Lett* 39(16):L16502.
8. Massonnet F, et al. (2012) Constraining projections of summer Arctic sea ice. *Cryosphere* 6:1383–1394.
9. Overland JE, Wang M (2013) When will the summer Arctic be nearly sea ice free? *Geophys Res Lett* 40(10):2097–2101.
10. Zhang R, Knutson TR (2013) The role of global climate change in the extreme low summer Arctic sea ice extent in 2012. *Bull Am Meteorol Soc* 94(9):S23–S26.
11. Francis JA, Hunter E (2006) New insight into the disappearing Arctic sea ice. *Eos Trans AGU* 87(46):509–511.
12. Deser C, Teng H (2008) Recent trends in Arctic sea ice and the evolving role of atmospheric circulation forcing, 1979–2007. *Arctic Sea Ice Decline: Observations, Projections, Mechanisms, and Implications*, Geophysical Monograph Series, eds DeWeaver ET, Bitz CM, Tremblay L-B (Am Geophys Union, Washington, DC), Vol 180, pp 7–26.
13. Steele M, Zhang J, Ermold W (2010) Mechanisms of summertime upper Arctic Ocean warming and the effect on sea ice melt. *J Geophys Res* 115(C11):C11004.
14. Winton M (2006) Amplified Arctic climate change: What does surface albedo feedback have to do with it? *Geophys Res Lett* 33(3):L03701.
15. Perovich DK, Richter-Menge JA, Jones KF, Light B (2008) Sunlight, water, and ice: Extreme Arctic sea ice melt during the summer of 2007. *Geophys Res Lett* 35(11):L11501.
16. Zhang J, Rothrock DA, Steele M (1998) Warming of the Arctic Ocean by a strengthened Atlantic inflow: Model results. *Geophys Res Lett* 25(10):1745–1748.
17. Polyakov IV, et al. (2010) Arctic Ocean warming contributes to reduced polar ice cap. *J Phys Oceanogr* 40(12):2743–2756.
18. Alexeev VA, Ivanov VV, Kwok R, Smedsrud LH (2013) North Atlantic warming and declining volume of Arctic sea ice. *Cryosphere Discuss* 7:245–265.
19. Woodgate RA, Weingartner TJ, Lindsay R (2012) Observed increases in Bering Strait oceanic fluxes from the Pacific to the Arctic from 2001 to 2011 and their impacts on the Arctic Ocean water column. *Geophys Res Lett* 39(24):L24603.
20. Rigor IG, Wallace JM (2004) Variations in the age of Arctic sea-ice and summer sea-ice extent. *Geophys Res Lett* 31(9):L09401.
21. Ogi M, Yamazaki K (2010) Trends in the summer Northern Annular Mode and Arctic sea ice. *SOLA* 6:41–44.
22. Shimada K, et al. (2006) Pacific Ocean inflow: Influence on catastrophic reduction of sea ice cover in the Arctic Ocean. *Geophys Res Lett* 33(8):L08605.
23. Proshutinsky AY, Johnson MA (1997) Two circulation regimes of the wind-driven Arctic Ocean. *J Geophys Res* 102(C6):12,493–12,514.
24. Wu B, Wang J, Walsh JE (2006) Dipole anomaly in the winter Arctic atmosphere and its association with sea ice motion. *J Clim* 19(2):210–225.
25. Wang J, et al. (2009) Is the Dipole Anomaly a major driver to record lows in Arctic summer sea ice extent? *Geophys Res Lett* 36(5):L05706.
26. Overland JE, Wang M (2010) Large-scale atmospheric circulation changes are associated with the recent loss of Arctic sea ice. *Tellus Ser A* 62(1):1–9.
27. Overland JE, Francis JA, Hanna E, Wang M (2012) The recent shift in early summer Arctic atmospheric circulation. *Geophys Res Lett* 39(19):L19804.
28. Wettstein JJ, Deser C (2014) Internal variability in projections of twenty-first century Arctic sea ice loss: Role of the large-scale atmospheric circulation. *J Clim* 27(2):527–550.
29. Deser C, Blackmon ML (1993) Surface climate variations over the North Atlantic Ocean during winter: 1900–1989. *J Clim* 6(9):1743–1753.
30. Park W, Latif M (2008) Multidecadal and multicentennial variability of the meridional overturning circulation. *Geophys Res Lett* 35(22):L22703.
31. Mahajan S, Zhang R, Delworth TL (2011) Impact of the Atlantic Meridional Overturning Circulation (AMOC) on Arctic surface air temperature and sea-ice variability. *J Clim* 24(24):6573–6581.
32. Day JJ, Hargreaves JC, Annan JD, Abe-Ouchi A (2012) Sources of multi-decadal variability in Arctic sea ice extent. *Environ Res Lett* 7(3):034011.
33. Miles MW, et al. (2014) A signal of persistent Atlantic multidecadal variability in Arctic sea ice. *Geophys Res Lett* 41(2):463–469.
34. Zhang R (2007) Anticorrelated multidecadal variations between surface and subsurface tropical North Atlantic. *Geophys Res Lett* 34(12):L12713.
35. Zhang R (2008) Coherent surface-subsurface fingerprint of the Atlantic meridional overturning circulation. *Geophys Res Lett* 35(20):L20705.
36. Delworth TL, et al. (2006) GFDL's CM2 global coupled climate models. Part I: Formulation and simulation characteristics. *J Clim* 19(5):643–674.
37. Nakamura N, Oort AH (1988) Atmospheric heat budgets of the polar regions. *J Geophys Res* 93(D8):9510–9524.
38. Beszczynska-Möller A, Woodgate RA, Lee C, Melling H, and Karcher M (2011) A synthesis of exchanges through the main oceanic gateways to the Arctic Ocean. *Oceanography* 24(3):82–99.
39. Holland MM, Bitz CM, Tremblay B, Bailey DA (2008) The role of natural versus forced change in future rapid summer Arctic ice loss. *Arctic Sea Ice Decline: Observations, Projections, Mechanisms, and Implications*, Geophysical Monograph Series, eds DeWeaver ET, Bitz CM, Tremblay L-B (Am Geophys Union, Washington, DC), Vol 180, pp 133–150.
40. Kay JE, Holland MM, Jahn A (2011) Inter-annual to multi-decadal Arctic sea ice extent trends in a warming world. *Geophys Res Lett* 38(15):L15708.
41. Bjerknes J (1964) *Atlantic Air-Sea Interaction*, Advances in Geophysics (Academic Press, New York), Vol 10, pp 1–82.
42. Koenigk T, Brodeau L (2014) Ocean heat transport into the Arctic in the twentieth and twenty-first century in EC-Earth. *Clim Dyn* 42:3101–3120.
43. Shaffrey L, Sutton R (2006) Bjerknes compensation and the decadal variability of the energy transports in a coupled climate model. *J Clim* 19(7):1167–1181.
44. Van der Swaluw E, Drijfhout SS, Hazeleger W (2007) Bjerknes compensation at high northern latitudes: The ocean forcing the atmosphere. *J Clim* 20(24):6023–6032.
45. Jungclaus JH, Koenigk T (2010) Low-frequency variability of the Arctic climate: the role of oceanic and atmospheric heat transport variations. *Clim Dyn* 34(2-3):265–279.
46. Årthun M, Eldevik T, Smedsrud LH, Skagseth Ø, Ingvaldsen RB (2012) Quantifying the influence of Atlantic heat on Barents Sea ice variability and retreat. *J Clim* 25(13):4736–4743.
47. Smedsrud LH, et al. (2013) The role of the Barents Sea in the Arctic climate system. *Rev Geophys* 51(3):415–449.
48. Winton M (2011) Do climate models underestimate the sensitivity of northern hemisphere sea ice cover? *J Clim* 24(15):3924–3934.
49. Fetterer F, Knowles K, Meier W, Savoie M (2002) *Sea Ice Index, 2000–2012* (Natl Snow Ice Data Cent, Boulder, CO) (updated daily).
50. Cavalieri DJ, Parkinson CL, Gloersen P, Zwally H (1996) *Sea Ice Concentrations from Nimbus-7 SMMR and DMSP SSMI-SSMIS Passive Microwave Data* (updated yearly) (Natl Snow Ice Data Cent, Boulder, CO).
51. Kalnay E, et al. (1996) The NCEP/NCAR 40-year reanalysis project. *Bull Am Meteorol Soc* 77(3):437–471.
52. Delworth TL, Zeng F (2012) Multicentennial variability of the Atlantic Meridional Overturning Circulation and its climatic influence in a 4000 year simulation of the GFDL CM2.1 climate model. *Geophys Res Lett* 39(13):L13702.